

HOI-Diff: Text-Driven Synthesis of 3D Human-Object Interactions using Diffusion Models

Xiaogang Peng^{1,2*}, Yiming Xie^{1*}, Zizhao Wu², Varun Jampani³, Deqing Sun⁴, Huaizu Jiang¹

¹Northeastern University, ²Hangzhou Dianzi University, ³Stability AI, ⁴Google Research

<https://neu-vi.github.io/HOI-Diff/>

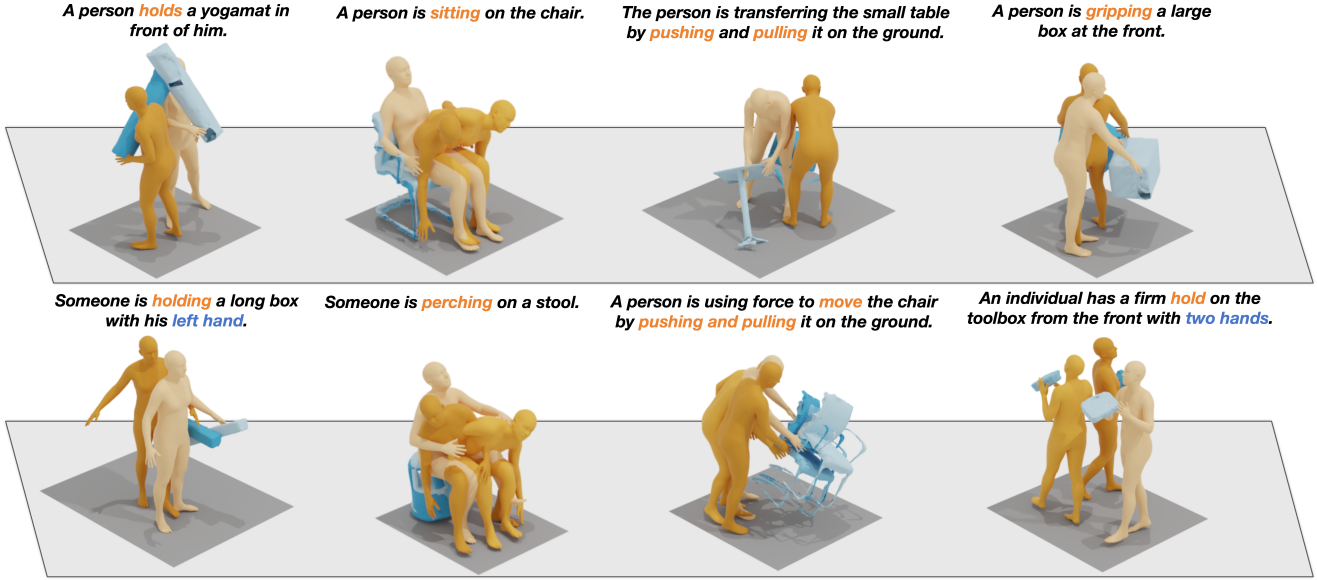


Figure 1. HOI-Diff can generate realistic motions for 3D human-object interactions given a text prompt and object geometry. Please see the supplementary material for video results. Darker color indicates later frames in the sequence. Best viewed in color.

Abstract

We address the problem of generating realistic 3D human-object interactions (HOIs) driven by textual prompts. Instead of a single model, our key insight is to take a modular design and decompose the complex task into simpler sub-tasks. We first develop a dual-branch diffusion model (HOI-DM) to generate both human and object motions conditioning on the input text, and encourage coherent motions by a cross-attention communication module between the human and object motion generation branches. We also develop an affordance prediction diffusion model (APDM) to predict the contacting area between the human and object during the interactions driven by the textual prompt. The APDM is independent of the results by the HOI-DM and thus can correct potential errors by the latter.

*Equal contribution.

Moreover, it stochastically generates the contacting points to diversify the generated motions. Finally, we incorporate the estimated contacting points into the classifier-guidance to achieve accurate and close contact between humans and objects. To train and evaluate our approach, we annotate BEHAVE dataset with text descriptions. Experimental results demonstrate that our approach is able to produce realistic HOIs with various interactions and different types of objects.

1. Introduction

Text-driven synthesis of 3D human-object interactions (HOIs) aims to generate motions for both the human and object that form coherent and semantically meaningful interactions. It enables virtual humans to naturally interact with objects, which has a wide range of applications in AR/VR,

video games, and filmmaking, etc.

The generation of natural and physically plausible 3D HOIs involves humans interacting with *dynamic* objects in *various* ways according to the text prompts, thereby posing several challenges. First, the variability of object shapes makes it particularly challenging to generate semantically meaningful contact between the human and objects to avoid floating objects. Second, the generated HOIs should be faithful to the input text prompts as there are many plausible interactions between human and the same object (*e.g.*, a person carries a chair, sits on a chair, pushes or pulls a chair). Text-driven 3D HOI synthesis with a diverse set of interactions is still under-explored. Third, the development and evaluation of 3D HOI synthesis models requires a high-quality human motion dataset with various HOIs and textual descriptions, but existing datasets lack either HOIs [10, 32] or textual descriptions [3].

On one hand, recent methods [11, 16, 22, 31, 40, 42, 49, 55] can synthesize realistic human motions for HOIs for *static* objects only. They usually synthesize the motion in the last mile of interaction, *i.e.* the motion between the given starting human pose and the final interaction pose, and overlook the movement of the objects when the human is interacting with them. On the other hand, existing methods for motion generation with dynamic objects do not adequately reflect the real-world complexity. For instance, they focus on grasping small objects [9], provide the object motion as conditioning [23], predict deterministic interactions between the human and the same object without the diversity [35, 51], consider only a small set of interactions (*e.g.* sit/lift [22], sit/lie down [11], sit [16, 31, 55], grasp [42, 49]), or investigate a single type of object (*e.g.* chair [16, 55]).

In this paper, we go beyond and propose **HOI-Diff** for 3D HOIs synthesis involving humans interacting with different types of objects in diverse ways, which are both physically plausible and semantically faithful to the textual prompt, as shown in Fig. 1. Our key insight is to decompose 3D HOIs synthesis into three modules: (a) **coarse 3D HOIs generation** that extends the human motion diffusion model [43] to a dual-branch diffusion model (HOI-DM) to generate both human and object motions conditioning on the input text prompt. To encourage coherent motions, we develop a cross-attention communication module, exchanging information between the human and object motion generation models; (b) **affordance prediction diffusion model** (APDM) that estimates the contacting points between the human and object during the interactions driven by the textual prompt. Our APDM does not rely on the results of the HOI-DM and thus can recover from its potential errors. Moreover, it stochastically generates the contacting points to diversity the generated motions; and (c) **affordance-guided interaction correction** that incorporates the esti-

mated contacting information and employs the classifier-guidance to achieve accurate and close contact between humans and objects, significantly alleviating the cases of floating objects. Compared with designing a monolithic model, our proposed HOI-Diff disentangles motion generation for humans and objects and estimation of their contacting points, which are later integrated to form coherent and diverse HOIs, reducing the complexity and burden for each of three modules.

To our best knowledge, HOI-Diff is the first text-driven approach capable of generating realistic motions for various HOIs and different types of objects during the interactions. For both training and evaluation purposes, we annotate each video sequence in BEHAVE dataset [3] with text descriptions, which bridges the gap of no data for text-driven 3D HOIs generation. Extensive experiments validate the effectiveness and design choices of our approach, particularly for dynamic objects, thereby enabling a set of new applications in human motion generation.

2. Related Work

Human Motion Generation with Diffusion Models. The denoising diffusion models have been widely used 2D image generations [34, 37, 38] and achieved impressive results. Recent work [1, 2, 4–6, 17, 36, 39, 41, 43, 44, 48, 50, 52–54, 56] apply the diffusion model in the task of human motion generation. While these methods have successfully generated human motion, they usually generate isolated motions in the free space without considering the objects the human is interacting with. Our method is primarily focused on motion generation with human-object interactions.

Scene- and Object-Aware Human Motion Generation. Recent works condition motion synthesis on scene geometry [14, 46, 47, 57]. This facilitates the understanding of human-scene interactions. However, the motion fidelity is compromised due to the lack of paired full scene-motion data. Other approaches [11, 16, 22, 31, 40, 55] instead focus on the interactions with the objects and can produce realistic motions. However, they focus on interacting with static objects with limited interactions. OMOMO [23] proposes a conditional diffusion framework that can generate full-body motion from the object motion. The object motion is needed as input in OMOMO, whereas our method can jointly synthesize human motion and object motion. IMoS [9] synthesizes the full-body human along with the 3D object motions from textual inputs. Although they can generate realistic interactions, IMoS only focuses on grasping small objects with hands. InterDiff [51] predicts whole-body interactions with dynamic objects. However, it focuses on the motion prediction task, where the future motion needs to be forecasted based on past motion information and object infor-

mation. Note that the interaction type is deterministic, given the object and past motion information. Different from this, we tackle the motion synthesis task, where the interaction with the same object can be controlled by the text prompt.

Multi-Human Motion Generation. Recent works [24, 39, 39] incorporate human-to-human interactions into the motion diffusion process. They usually also adopt cross-attention to exchange information from different human motions. Different from them, our goal is to generate coarse HOIs instead of doing so in a single run, which alleviates the burden of the model.

Affordance Estimation. The affordance estimation on 3D point cloud is studied in [7, 15, 19–21, 27, 28]. [19] formulates this task as the point cloud segmentation task from the extracted geometric features. [20] voxelizes the point cloud and creates affordance maps with interactive manipulation. [15, 21] focuses on the object grasping affordances and some specific applications. [27] learns the affordance for object-object interactions. [28] addressed the task of open-vocabulary affordance learning. Overall affordance learning is a very challenging task even the shape of point cloud is given. Instead of predicting the point-wise contact labels, in our method, we propose to make some hypotheses to simplify human-object interactions, making it more tractable without significantly compromising accuracy.

3. Method

3.1. Overview

Motion Representations. We denote a 3D HOI sequence as $\mathbf{x} = \{\mathbf{x}^h, \mathbf{x}^o\}$. It consists of human motion sequence $\mathbf{x}^h \in \mathbb{R}^{L \times D^h}$ and object motion sequence $\mathbf{x}^o \in \mathbb{R}^{L \times D^o}$, where L denotes the length of the sequence. For \mathbf{x}^h , we adopt the redundant representation widely used in human motion generation [10] with $D^h = 263$, which include pelvis velocity, local joint positions, velocities and rotations of other joints in the pelvis space, and binary foot-ground contact labels. For the object motion sequence \mathbf{x}^o , we assume the object geometry is given as an input, and thus we only need to estimate its 6DoF poses in the generation, *i.e.*, $D^o = 6$. We represent each object instance as a point cloud of 512 points $\mathbf{p} \in \mathbb{R}^{512 \times 3}$.

Diffusion Model for 3D HOI Generation. Given a prompt $\mathbf{c} = (\mathbf{d}, \mathbf{p})$, consisting of a textual description \mathbf{d} and the object instance’s point cloud \mathbf{p} , a diffusion model $p_\theta(\mathbf{x}_{t-1}|\mathbf{x}_t, \mathbf{c})^*$ learns the reverse diffusion process to generate clean data from a Gaussian noise \mathbf{x}_t with T consecutive denoising steps

$$p_\theta(\mathbf{x}_{t-1}|\mathbf{x}_t, \mathbf{c}) := \mathcal{N}(\mathbf{x}_{t-1}, \mu_\theta(\mathbf{x}_t, t, \mathbf{c}), (1 - \alpha_t)\mathbf{I}), \quad (1)$$

*We use superscripts h and o to denote human and object sequence, respectively. Without a superscript, it means the 3D HOI sequence, containing both \mathbf{x}^h and \mathbf{x}^o . Subscript is used for the diffusion denoising step.

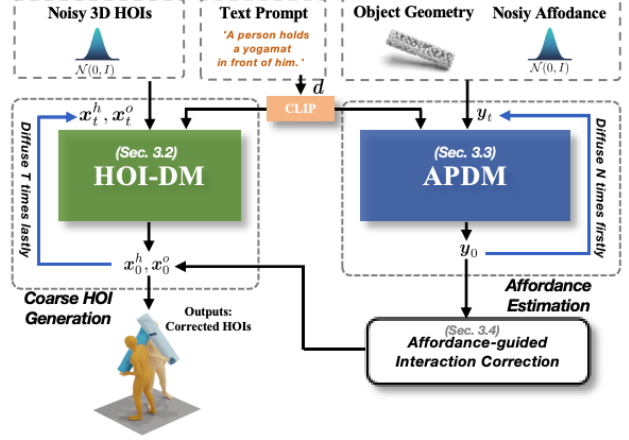


Figure 2. **Overview of HOI-Diff for 3D HOIs generation using diffusion models.** Our key insight is to decompose the generation task into three modules: (a) coarse 3D HOI generation using a dual-branch diffusion model (HOI-DM), (b) affordance prediction diffusion model (APDM) to estimate the contacting points of humans and objects, and (c) affordance-guided interaction correction, which incorporates the estimated contacting information and employs the classifier-guidance to achieve accurate and close contact between humans and objects to form coherent HOIs.

where t is the denoising step. Following [43], instead of predicting the noise ϵ_t in each diffusion step, our diffusion model M_θ with parameters θ predicts the final clean motion $\mathbf{x}_0 = M_\theta(\mathbf{x}_t, t, \mathbf{c})$. We sample $\mathbf{x}_{t-1} \sim \mathcal{N}(\mu_t, \Sigma_t)$ and compute the mean as in [29]

$$\mu_t = \frac{\sqrt{\alpha_{t-1}}\beta_t}{1 - \alpha_t}\mathbf{x}_0 + \frac{\sqrt{1 - \beta_t}(1 - \alpha_{t-1})}{1 - \alpha_t}\mathbf{x}_t, \quad (2)$$

where $\alpha_t = \prod_{s=1}^t(1 - \beta_s)$ and $\beta_t \in (0, 1)$ are the variance schedule. $\Sigma_t = \frac{1 - \alpha_{t-1}}{1 - \alpha_t}\beta_t$ [13] is a variance scheduler of choice. Similar to \mathbf{x}_t , μ_t consists of μ_t^h and μ_t^o , corresponding to human and object motion, respectively.

Simply adopting the diffusion model described in Eq.(1) would impose huge burden to the model, which requires joint generation of human and object motion and more critically, enforcement of their intricate interactions to follow the input textual description. In this paper, we propose **HOI-Diff** for 3D HOIs generation, which disentangles motion generation for humans and objects and estimation of their contacting points, which are later integrated to form coherent and diverse HOIs, reducing the complexity and burden for each of three modules. Fig. 2 shows the overview of our proposed approach. We introduce a dual-branch Human-Object Interaction Diffusion Model (HOI-DM), which can produce diverse yet consistent motions, capturing the intricate interplay and mutual interactions between humans and objects (Sec. 3.2). To ensure physically plausible contact between humans and objects,

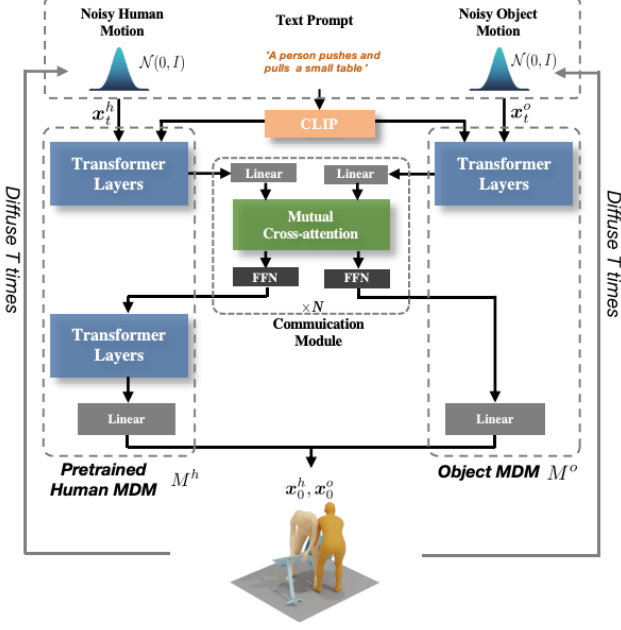


Figure 3. **Illustration of HOI-DM architecture for coarse 3D HOIs generation.** It has two branches designed for generating human and object motions individually. A mutual cross-attention is introduced to allow information exchange between two branches to generate coherent motions.

we propose a novel affordance prediction diffusion model (APDM) (Sec. 3.3), whose output will be used as classifier guidance (Sec. 3.4) to correct the interactions at each diffusion step of human/object motion generation.

3.2. Coarse 3D HOIs Generation

First, we introduce a dual-branch Human-Object Interaction Diffusion Model (HOI-DM) to generate human and object motions that are roughly coherent. As shown in Fig. 3, it consists of two Transformer models [45], human motion diffusion model (MDM) M^h and object MDM M^o , which work similar to [43]. Specifically, at the diffusion step t , they take the text description and noisy motions x_t^h and x_t^o as input and predicts clean human and object motions x_0^h and x_0^o , respectively.

To enhance the learning of interactions of the human and object when generating their motion, we introduce a Communication Module (CM) designed for exchanging feature representations between the human MDM M^h and the object MDM M^o . CM is a Transformer block that receives the intermediate feature f^h, f^o from both M^h and M^o . It then processes these inputs to generate refined updates based on the cross attention mechanism [45]. The updated feature representations \hat{f}^h and \hat{f}^o of the human and object are then conditioned on each other, which are then fed into the subsequent layers of their respective branches to esti-

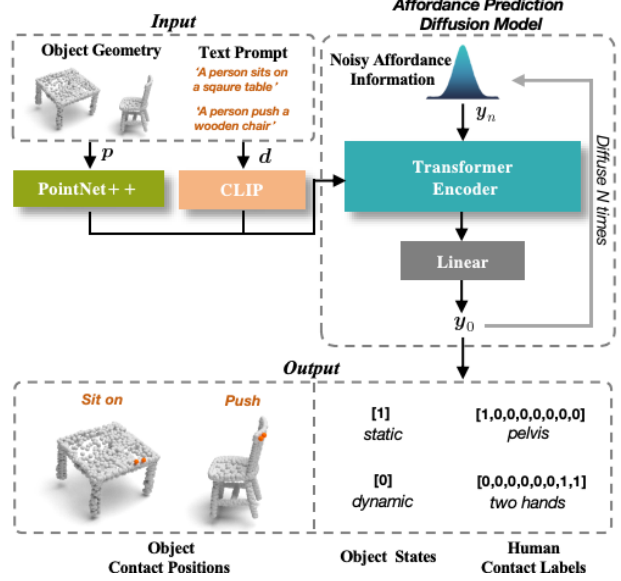


Figure 4. **Illustration of APDM architecture for affordance estimation.** Affordance information of human contact labels, object contact positions, and binary object states are represented together as a noise variable, which is fed into the Transformer encoder to generate clean affordance estimation. The object point cloud and textual prompt are taken as conditional input.

mate clean human and object motion x_0^h and x_0^o , respectively. The CM is inserted at the 4th transformer layer for human MDM and the last layer for object MDM, which was empirically found to work better.

Given the limited data availability for 3D HOI generation, during training, the human motion model M^h fine-tunes a pretrained human MDM [43]. This fine-tuning is critical to ensure the smoothness of the generated human motions. We ablate this design choice in Sec. 4.3.

3.3. Affordance Estimation

Due to the complexity of the interactions between a human and object, HOI-DM alone usually fails to produce physically plausible results, leading to floating objects or penetrations. To improve the generation of intricate interactions, the first problem that needs to be solved is to *identify where the contacting areas are* between the human and object. InterDiff [51] defines the contacting area based on the distance measurement between the surface of human and object. This approach, however, heavily relies on the quality of the generated human and object motions and cannot recover from errors in the coarse 3D HOI results. In addition, the contact area is diverse even with the same object and interaction type, e.g., “sit” can happen on either side of a table. To this end, we introduce an Affordance Prediction Diffusion Model (APDM) for affordance estimation. As illustrated in Fig. 4, the input to this model includes a

text description d and the object point cloud p . Our APDM doesn't rely on the results of the HOI-DM and thus can recover from the potential errors in HOI-DM. In addition, it stochastically generates the contacting points to ensure the diversity of the generated motions.

Affordance estimation in 3D point clouds itself is a notably challenging problem [7, 15, 19–21, 27, 28], especially in the context of 3D HOI generation involving textual prompt. To address the limited availability of training data, we propose a simplified approach that diverges from predicting point-wise contact labels. Our method is grounded in two key hypotheses. Firstly, we posit that interactions with an object involve a maximum of two contact points. Secondly, we identify eight primary body joints – the pelvis, neck, feet, shoulders, and hands – as the primary interacting parts in most HOI scenarios. These hypotheses streamline the complexity of the problem, making it more tractable without significantly compromising accuracy. For instance, this approach effectively models common interactions such as grasping an object with both hands, sitting actions involving the pelvis, or lifting with a single hand. Our empirical observations suggest that these simplifications are valid in a wide range of HOI applications, providing a balance between model complexity and real-world applicability.

Specifically, at each diffusion time step n of APDM², the noisy affordance data y_n includes human contact labels $y_n^h \in \{0, 1\}^8$, two object contact positions $y_n^o \in \mathbb{R}^{2 \times 3}$. In addition, our APDM also generates a binary object state label $y_n^s \in \{0, 1\}$ indicating whether it remains static or moves during the interaction. The generated binary label can help us better process static objects when synthesizing 3D HOIs, as discussed in the following section. APDM works similar to the diffusion denoising process described in Eq.(1). Its output include clean affordance information $y_0 = (y_0^h, y_0^o, y_0^s)$.

3.4. Affordance-guided Interaction Correction

With the estimated affordance, we can better align human and object motions to form coherent interactions. To this end, we propose to use the classifier guidance [8] to achieve accurate and close contact between humans and objects, significantly alleviating the cases of floating objects.

Specifically, in a nutshell, we define an analytic function $G(\mu_t^h, \mu_t^o, y_0)$ that assesses how closely the generated human joints and object's 6DoF pose align with a desired objective. In our case, it enforces the contact positions of human and object to be close to each other and their motions are smooth temporally. Based on the gradient of $G(\mu_t^h, \mu_t^o, y_0)$, we can perturb the generated human and

Algorithm 1 Affordance-guided Interaction Correction

Require: Input $c = (d, p)$ consisting of a textual description d and object point cloud p , HOI-Diff model M_θ , objective function $G(\mu_t^h, \mu_t^o, y_0)$, and estimated affordance $y_0 = (y_0^h, y_0^o, y_0^s)$.

```

1:  $x_T^h, x_T^o \leftarrow \text{sample from } \mathcal{N}(0, \mathbf{I})$ 
2:  $K = 1$ 
3: for all  $t$  from  $T$  to 1 do
4:    $x_0^h, x_0^o \leftarrow M_\theta(x_t^h, x_t^o, t, c)$ 
5:   Get  $\mu_t^h, \mu_t^o$  according to Eq.(2) with  $\Sigma_t$ 
6:   if  $t = 1$  then
7:      $K = 100$ 
8:   end if
9:   for all  $k$  from  $K$  to 1 do
10:     $\mu_t^h \leftarrow \mu_t^h - \tau_1 \Sigma_t \nabla_{\mu_t^h} G(\mu_t^h, \mu_t^o, y_0)$ 
11:     $\mu_t^o \leftarrow \mu_t^o - \tau_2 \Sigma_t \nabla_{\mu_t^o} G(\mu_t^h, \mu_t^o, y_0)$ 
12:   end for
13:    $x_{t-1}^h \sim \mathcal{N}(\mu_t^h, \Sigma_t)$ 
14:    $x_{t-1}^o \sim \mathcal{N}(\mu_t^o, \Sigma_t)$ 
15: end for
16: return  $x_0^h, x_0^o$ 
```

object motion at each diffusion step t as in [18, 22, 50],

$$\mu_t^h = \mu_t^h - \tau_1 \Sigma_t \nabla_{\mu_t^h} G(\mu_t^h, \mu_t^o, y_0), \quad (3)$$

$$\mu_t^o = \mu_t^o - \tau_2 \Sigma_t \nabla_{\mu_t^o} G(\mu_t^h, \mu_t^o, y_0). \quad (4)$$

Here τ_1 and τ_2 are different strengths to control the guidance for human and object motion, respectively. Due to the sparseness of object motion features, we assign a larger value to τ_2 compared to τ_1 . This applies greater strength to perturb object motion, facilitating feasible corrections for contacting joints. During the denoising stage, to eliminate diffusion models' bias that can suppress the guidance signal, we iteratively perturb K times in the last denoising step, as illustrated in Algorithm 1.

How can we define the objective function $G(\mu_t^h, \mu_t^o, y_0)$? We consider three terms here. First, in the generated 3D HOIs, the human and object should be close to each other on the contacting points. We therefore minimize the distance between human contact joints and object contact points

$$G_{con} = \sum_{i \in \{1, 2\}} \|R(\mu_t^h(i)) - V(y_t^o(i))\|^2, \quad (5)$$

where $\mu_t^h(i)$ and $y_t^o(i)$ denote the i -th contacting joint indexed by y_0^h and i -th object contact point, respectively. If there is just a single predicted contacting joint, $i = 1$. $R(\cdot)$ converts the human joint's local positions to global absolute locations, and $V(\cdot)$ obtains the object's contact point sequence from the predicted mean of object pose μ_t^o .

²We note that APDM and HOI-DM work independently. We thus use two symbols to denote the different diffusion time steps to avoid confusion.

Second, the generated motion of dynamic objects typically follows human movement. However, we observe that when the human interacts with a static object, such as sitting on a chair, the object appears slightly moved. To address this, we utilize the predicted object states y_0^s to immobilize the object’s movement in the generated samples if the state is static, ensuring that proper contact is established between the human and the static object. The objective is defined as

$$G_{sta} = \sum_{l=1}^L y_0^s(l) \|\mu_t^o(l) - \bar{\mu}_t^o\|^2, \quad (6)$$

where $\mu_t^o(l)$ denotes the object’s 6DoF pose in the l -th frame. $\bar{\mu}_t^o = \frac{1}{L} \sum_l \mu_t^o(l)$, which is the average of predicted means of the object’s pose.

Third, we define a smoothness term $G_{smo}(\mu)$ for the object motion to mitigate motion jittering during contact. Due to space limit, we explain it in the supplementary material.

Finally, we combine all these goal functions to as the final objective

$$G = G_{cont} + \alpha G_{sta} + \beta G_{smo}, \quad (7)$$

where α and β are weights for balance.

4. Experiments

4.1. Setup

Dataset. Since no dataset exists designed for studying text-driven 3D HOIs generation, we manually label interaction types, interacting subjects, and contact body parts on top of the BEHAVE dataset [3]. We then use ChatGPT to assist in generating three text descriptions for each HOI sequence, increasing the diversity of the data. Specifically, BEHAVE encompasses the interactions of 8 subjects with 20 different objects. It provides the human SMPL-H representation [25], the object mesh, as well as its 6DoF pose information in each HOI sequence. To ensure consistency in our approach, we follow the processing method used in HumanML3D [10] to extract representations for 22 body joints. All the models are trained to generate $L = 196$ frames in our experiments. In the end, we have 1451 3D HOI sequences along with textual descriptions to train and evaluate our proposed approach. We provide more details in the supplementary material.

Evaluation metrics. We first assess different models for human motion generation using standard metrics as introduced by [10], namely *Fréchet Inception Distance (FID)*, *R-Precision*, and *Diversity*. *FID* quantifies the discrepancy between the distributions of actual and generated motions via a pretrained motion encoder. *R-Precision* gauges the relevance between generated motions and their corresponding text prompts. *Diversity* evaluates the range of variation in the generated motions. Additionally, we compute

the *Foot Skating Ratio* to measure the proportion of frames exhibiting foot skid over a threshold (2.5 cm) during ground contact (foot height < 5 cm).

To evaluate the effectiveness of HOIs generation, we report the *Contact Distance* metric, which quantitatively measures the proximity between the ground-truth human contact joints and the object contact points. Ideally, we should develop similar metrics, *e.g.*, *FID*, to evaluate the *stochastic* HOI generation. However, due to the limited data available in BEHAVE [3], training a motion encoder would produce biased evaluation results. To mitigate this issue, we resort to user studies to quantify the effectiveness of different models. Details will be introduced later.

4.2. Comparisons with Existing Methods

Baselines. As our work introduces a novel 3D HOIs generation task not addressed by existing text-to-motion methods, which focus exclusively on human motion generation without accounting for human-object interactions. To compare with existing works, we mainly focus on evaluating human motion generation. We then design different variants of our models for comparing 3D HOIs generation. Specifically, we adopt the prominent text-to-motion methods MDM [43] and PriorMDM* [39] with the following settings. (a) MDM^{finetuned}: In this setup, we fine-tune the original MDM model [43] on the BEHAVE dataset [3]. (b) MDM*: This variant involves adapting the input and output layers’ dimensions of the MDM model [43] to accommodate the input of 3D HOI sequences. This adjustment allows for the simultaneous learning of both human and object motions within a singular, integrated model. (c) PriorMDM* [39]: We adapt the ComMDM architecture proposed in [39], originally designed for two-person motion generation, to suit our needs for HOIs synthesis by modifying one of its two branches for object motion generation. More details are provided in the supplementary material.

Quantitative Results. Tab. 1 reports the quantitative results on BEHAVE dataset [3]. Compared with the baseline methods, our full method achieves the best performance. Specifically, it achieves state-of-the-art results in both *FID*, *R-precision*, and *Diversity* underscoring its ability to generate high-quality human motions in the context of coherently interacting with objects. The best *Contact Distance* also suggests that our approach can generate physically plausible HOIs, capturing the intricate interplay and mutual interactions between humans and objects.

We also show the results of our *User Study* in Tab. 1 to illustrate user preferences between our method and other baselines. In our user study, we sample 12 sequences from each method and participants are asked to choose their most preferred generation results from these samples. This user study is designed to directly compare user preferences across different methods. The result indicates a strong pref-

Table 1. **Quantitative results on the BEHAVE [3] dataset.** We compare our method with three baselines adapted from existing models and the real data. The right arrow \rightarrow means closer to real data is better.

	FID \downarrow	R-precision \uparrow (Top-3)	Diversity \rightarrow	Contact Distance \downarrow	Foot Skate Ratio \downarrow	User Study \uparrow (preferred)
Real	0.096	0.324	7.244	-	-	-
MDM ^{finetuned} [43]	3.832	0.198	7.976	-	-	-
MDM* [43]	3.169	0.206	7.606	0.448	0.184	1.20%
PriorMDM* [39]	4.352	0.215	8.186	0.416	0.270	21.42%
Ours (Full)	1.632	0.222	7.596	0.363	0.190	77.38%

Table 2. **Ablation studies of our model’s variants on the BEHAVE dataset.** The right arrow \rightarrow means closer to real data is better.

	FID \downarrow	R-precision \uparrow (Top-3)	Diversity \rightarrow	Contact Distance \downarrow	Foot Skate Ratio \downarrow	User Study \uparrow (preferred)
<i>w/o Interaction Correction</i>						
Ours w/o CM	2.825	0.201	7.850	0.524	0.265	0.00%
Ours w/o pretrain	2.414	0.226	7.915	0.402	0.158	3.90%
Ours ^{global}	11.057	0.187	7.545	0.375	0.274	0.00%
Ours	1.808	0.217	7.718	0.416	0.205	11.69%
<i>w/ Interaction Correction</i>						
Ours w/o M^o & CM	3.206	0.205	7.909	0.365	0.310	0.00%
Ours w/o G_{con}	1.983	0.205	7.826	0.417	0.196	-
Ours w/o G_{sta}	1.636	0.213	7.785	0.367	0.181	-
Ours w/o G_{smo}	1.665	0.205	7.840	0.370	0.182	-
Ours (Full)	1.632	0.222	7.596	0.363	0.190	84.41%

erence for our method: it is favored over the baselines in a substantial majority of 77.38% of the cases.

Qualitative Results. We showcase qualitative comparisons between our approach and the baseline methods in Fig. 5. After rendering with SMPL [25] shapes, it is observed that the generated HOI motion by other baselines lacks smoothness and realism, where the object may float in the air (e.g., the toolbox in Fig. 5 (b)). Furthermore, these baseline methods struggle to accurately capture the spatial relationships between humans and objects (e.g., the chair in Fig. 5 (e)). In stark contrast, our approach excels in creating visually appealing and realistic HOIs. Notably, it adeptly reflects the intricate details outlined in text descriptions, capturing both the nature of the interactive actions and the specific body parts involved (e.g., raising the trash bin with the right hand in Fig. 5 (a)).

4.3. Ablation Studies

We conduct extensive ablation studies in Tab. 2 and Fig. 6 to validate the effectiveness of different components in our method. Tab. 2 categorizes the results into two parts depending on whether to use the affordance-guided interaction correction introduced in Sec. 3.4: *w/o Interaction Correction* and *w/ Interaction Correction*.

w/o Interaction Correction. In this part, we remove the affordance-guided interaction correction in the inference stage and compare each ablated variant with our method. When the Communication Module (CM) in HOI-DM is

disabled, all the results drop substantially, especially in *Contact Distance*. “Ours w/o pretrain” demonstrates the effectiveness of fine-tuning the pretrained MDM [43] for human motion generation. Furthermore, as illustrated in “Ours^{global}”, although we could also represent human joints in the same global space as the object 6DoF pose, we empirically find that the hybrid combination of the human joints articulated in a local coordinate system and the object pose defined in a global space works better.

w/ Interaction Correction. A straightforward approach of generating 3D HOIs can be generating only human motion first and subsequently binding the object to the human body. To validate this design, we eliminate M^o and CM in HOI-DM from our training process, focusing solely on learning human motion. During inference, we apply the affordance-guided interaction correction to align the object motion with the human. However, as shown in the Tab. 2, it affects human motion performance, yielding unsatisfactory results. We also evaluate the effectiveness of the three analytic functions used in our interaction correction process. Notably, the function G_{con} , which incorporates the estimated affordance information to ensure close contact between humans and objects, prove to be crucial for generating realistic HOIs. The results clearly demonstrate the significance of affordance estimation in enhancing the authenticity of the interactions.

In addition to our primary quantitative evaluations, we also conduct *User Study* for ablation analysis. The results

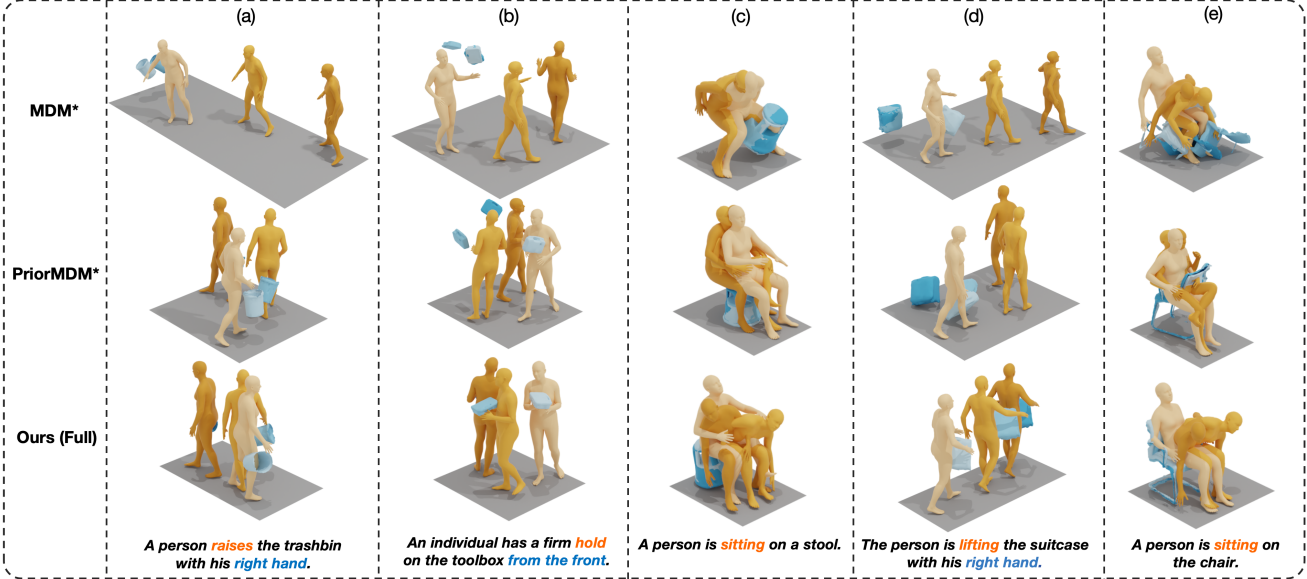


Figure 5. **Qualitative comparisons of our approach and baseline methods.** The bottom row, showcasing our method, demonstrates the generation of realistic 3D HOIs with plausible contacts, particularly evident in columns 2 and 4. This contrasts with the baselines, which fail to achieve a similar level of realism and contact plausibility in the interactions. As an additional visual aid, the mesh color gradually darkens over time to represent progression. (Best viewed in color.)

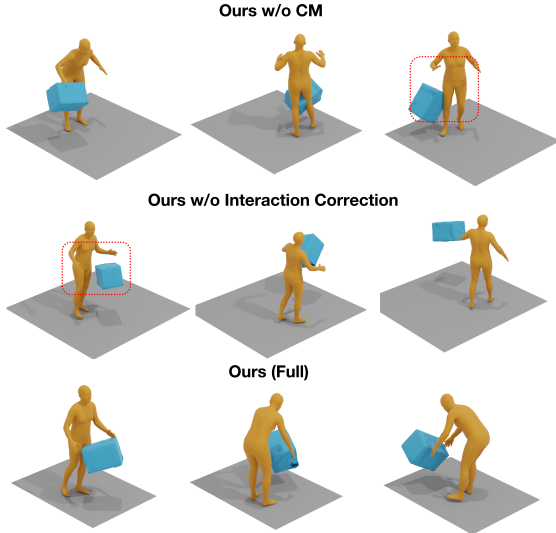


Figure 6. **Visual results of different variants of our model in ablation studies on the BEHAVE dataset [3].**

from this study indicate a clear user preference for our full method. This preference is observed consistently across various variants, underscoring the effectiveness of the complete set of design choices in our approach.

4.4. Limitations

The existing datasets for 3D HOIs are limited in terms of action and motion diversity, posing a challenge for syn-

thesizing long-term interactions in our task. Furthermore, the effectiveness of our model’s interaction correction component is contingent on the precision of affordance estimation. Despite simplifying this task, achieving accurate affordance estimation remains a significant challenge, impacting the overall performance of our model. A promising direction for future research involves integrating a sophisticated affordance model pre-trained on an extensive 3D object dataset, along with text prompts. Such an advancement could significantly enhance the realism and accuracy of human-object contact in our model, leading to more natural and precise HOIs synthesis.

5. Conclusion

In summary, we presented a novel approach HOI-Diff to generate realistic 3D HOIs driven by textual prompts. By employing a modular design, we effectively decompose the complex task of HOI synthesis into simpler sub-tasks, enhancing the coherence and realism of the generated motions. Our HOI-Diff model successfully generates coarse dynamic human and object motions, while the affordance prediction diffusion model adds precision in predicting contact areas. The integration of estimated affordance data into classifier-guidance further ensures accurate human-object interactions. The promising experimental results on our annotated BEHAVE dataset demonstrate the efficacy of our approach in producing diverse and realistic HOIs.

References

- [1] Hyemin Ahn, Esteve Valls Mascaro, and Dongheui Lee. Can we use diffusion probabilistic models for 3d motion prediction? *arXiv preprint arXiv:2302.14503*, 2023. 2
- [2] German Barquero, Sergio Escalera, and Cristina Palmero. Belfusion: Latent diffusion for behavior-driven human motion prediction. In *Proceedings of the IEEE/CVF International Conference on Computer Vision*, pages 2317–2327, 2023. 2
- [3] Bharat Lal Bhatnagar, Xianghui Xie, Ilya Petrov, Cristian Sminchisescu, Christian Theobalt, and Gerard Pons-Moll. Behave: Dataset and method for tracking human object interactions. In *IEEE Conference on Computer Vision and Pattern Recognition (CVPR)*. IEEE, 2022. 2, 6, 7, 8, 1, 3
- [4] Ling-Hao Chen, Jiawei Zhang, Yewen Li, Yiren Pang, Xiaobo Xia, and Tongliang Liu. Humanmac: Masked motion completion for human motion prediction. *arXiv preprint arXiv:2302.03665*, 2023. 2
- [5] Xin Chen, Biao Jiang, Wen Liu, Zilong Huang, Bin Fu, Tao Chen, and Gang Yu. Executing your commands via motion diffusion in latent space. In *CVPR*, 2023.
- [6] Rishabh Dabral, Muhammad Hamza Mughal, Vladislav Golyanik, and Christian Theobalt. Mofusion: A framework for denoising-diffusion-based motion synthesis. In *CVPR*, 2023. 2
- [7] Shengheng Deng, Xun Xu, Chaozheng Wu, Ke Chen, and Kui Jia. 3d affordancenet: A benchmark for visual object affordance understanding. In *Proceedings of the IEEE Conference on Computer Vision and Pattern Recognition*, 2021. 3, 5
- [8] Prafulla Dhariwal and Alexander Nichol. Diffusion models beat gans on image synthesis. In *NeurIPS*, 2021. 5
- [9] Anindita Ghosh, Rishabh Dabral, Vladislav Golyanik, Christian Theobalt, and Philipp Slusallek. Imos: Intent-driven full-body motion synthesis for human-object interactions. In *CGF*, 2023. 2
- [10] Chuan Guo, Shihao Zou, Xinxin Zuo, Sen Wang, Wei Ji, Xingyu Li, and Li Cheng. Generating diverse and natural 3d human motions from text. In *CVPR*, 2022. 2, 3, 6
- [11] Mohamed Hassan, Duygu Ceylan, Ruben Villegas, Jun Saito, Jimei Yang, Yi Zhou, and Michael Black. Stochastic scene-aware motion prediction. In *ICCV*, 2021. 2
- [12] Dan Hendrycks and Kevin Gimpel. Gaussian error linear units (gelus). *arXiv preprint arXiv:1606.08415*, 2016. 2
- [13] Jonathan Ho, Ajay Jain, and Pieter Abbeel. Denoising diffusion probabilistic models. 2020. 3
- [14] Siyuan Huang, Zan Wang, Puhao Li, Baoxiong Jia, Tengyu Liu, Yixin Zhu, Wei Liang, and Song-Chun Zhu. Diffusion-based generation, optimization, and planning in 3d scenes. In *CVPR*, 2023. 2
- [15] Ander Iriondo, Elena Lazkano, and Ander Ansuategi. Affordance-based grasping point detection using graph convolutional networks for industrial bin-picking applications. *Sensors*, 21(3):816, 2021. 3, 5
- [16] Nan Jiang, Tengyu Liu, Zhexiong Cao, Jieming Cui, Yixin Chen, He Wang, Yixin Zhu, and Siyuan Huang. Chairs: Towards full-body articulated human-object interaction. *ArXiv*, 2022. 2
- [17] Korrawe Karunratanakul, Konpat Preechakul, Supasorn Suwajanakorn, and Siyu Tang. Gmd: Controllable human motion synthesis via guided diffusion models. In *ICCV*, 2023. 2
- [18] Korrawe Karunratanakul, Konpat Preechakul, Supasorn Suwajanakorn, and Siyu Tang. Guided motion diffusion for controllable human motion synthesis. In *Proceedings of the IEEE/CVF International Conference on Computer Vision*, pages 2151–2162, 2023. 5
- [19] David Inkyu Kim and Gaurav S Sukhatme. Semantic labeling of 3d point clouds with object affordance for robot manipulation. In *2014 IEEE International Conference on Robotics and Automation (ICRA)*, pages 5578–5584. IEEE, 2014. 3, 5
- [20] David Inkyu Kim and Gaurav S Sukhatme. Interactive affordance map building for a robotic task. In *2015 IEEE/RSJ International Conference on Intelligent Robots and Systems (IROS)*, pages 4581–4586. IEEE, 2015. 3
- [21] Mia Kokic, Johannes A Stork, Joshua A Haustein, and Danica Kragic. Affordance detection for task-specific grasping using deep learning. In *2017 IEEE-RAS 17th International Conference on Humanoid Robotics (Humanoids)*, pages 91–98. IEEE, 2017. 3, 5
- [22] Nilesh Kulkarni, Davis Rempe, Kyle Genova, Abhijit Kundu, Justin Johnson, David Fouhey, and Leonidas Guibas. Nifty: Neural object interaction fields for guided human motion synthesis. *ArXiv*, 2023. 2, 5
- [23] Jiaman Li, Jiajun Wu, and C Karen Liu. Object motion guided human motion synthesis. *arXiv preprint arXiv:2309.16237*, 2023. 2
- [24] Han Liang, Wenqian Zhang, Wenxuan Li, Jingyi Yu, and Lan Xu. Intergen: Diffusion-based multi-human motion generation under complex interactions. *arXiv*, 2023. 3
- [25] Matthew Loper, Naureen Mahmood, Javier Romero, Gerard Pons-Moll, and Michael J. Black. SMPL: A skinned multi-person linear model. *ACM Trans. Graphics (Proc. SIGGRAPH Asia)*, 34(6):248:1–248:16, 2015. 6, 7
- [26] Ilya Loshchilov and Frank Hutter. Decoupled weight decay regularization. In *ICLR*, 2017. 2
- [27] Kaichun Mo, Yuzhe Qin, Fanbo Xiang, Hao Su, and Leonidas Guibas. O2o-afford: Annotation-free large-scale object-object affordance learning. In *Conference on Robot Learning*, pages 1666–1677. PMLR, 2022. 3, 5
- [28] Toan Ngyen, Minh Nhat Vu, An Vuong, Dung Nguyen, Thieu Vo, Ngan Le, and Anh Nguyen. Open-vocabulary affordance detection in 3d point clouds. *arXiv preprint arXiv:2303.02401*, 2023. 3, 5
- [29] Alexander Quinn Nichol and Prafulla Dhariwal. Improved denoising diffusion probabilistic models. In *ICML*, 2021. 3
- [30] Adam Paszke, Sam Gross, Francisco Massa, Adam Lerer, James Bradbury, Gregory Chanan, Trevor Killeen, Zeming Lin, Natalia Gimelshein, Luca Antiga, et al. Pytorch: An imperative style, high-performance deep learning library. *Advances in neural information processing systems*, 32, 2019. 2

- [31] Huaijin Pi, Sida Peng, Minghui Yang, Xiaowei Zhou, and Hujun Bao. Hierarchical generation of human-object interactions with diffusion probabilistic models. In *ICCV*, 2023. 2
- [32] Matthias Plappert, Christian Mandery, and Tamim Asfour. The kit motion-language dataset. *Big Data*, 2016. 2
- [33] Charles Ruizhongtai Qi, Li Yi, Hao Su, and Leonidas J Guibas. Pointnet++: Deep hierarchical feature learning on point sets in a metric space. *Advances in neural information processing systems*, 30, 2017. 1
- [34] Aditya Ramesh, Mikhail Pavlov, Gabriel Goh, Scott Gray, Chelsea Voss, Alec Radford, Mark Chen, and Ilya Sutskever. Zero-shot text-to-image generation. In *ICML*, 2021. 2
- [35] Haziq Razali and Yiannis Demiris. Action-conditioned generation of bimanual object manipulation sequences. In *Proceedings of the AAAI Conference on Artificial Intelligence*, pages 2146–2154, 2023. 2
- [36] Davis Remppe, Zhengyi Luo, Xue Bin Peng, Ye Yuan, Kris Kitani, Karsten Kreis, Sanja Fidler, and Or Litany. Trace and pace: Controllable pedestrian animation via guided trajectory diffusion. In *CVPR*, 2023. 2
- [37] Robin Rombach, Andreas Blattmann, Dominik Lorenz, Patrick Esser, and Björn Ommer. High-resolution image synthesis with latent diffusion models. In *CVPR*, 2022. 2
- [38] Chitwan Saharia, William Chan, Saurabh Saxena, Lala Li, Jay Whang, Emily L Denton, Kamyar Ghasemipour, Raphael Gontijo Lopes, Burcu Karagol Ayan, Tim Salimans, et al. Photorealistic text-to-image diffusion models with deep language understanding. In *NeurIPS*, 2022. 2
- [39] Yonatan Shafir, Guy Tevet, Roy Kapon, and Amit H. Bermano. Human motion diffusion as a generative prior. *ArXiv*, 2023. 2, 3, 6, 7
- [40] Sebastian Starke, He Zhang, Taku Komura, and Jun Saito. Neural state machine for character-scene interactions. *TOG*, 2019. 2
- [41] Jiarui Sun and Girish Chowdhary. Towards globally consistent stochastic human motion prediction via motion diffusion. *arXiv preprint arXiv:2305.12554*, 2023. 2
- [42] Omid Taheri, Vasileios Choutas, Michael J. Black, and Dimitrios Tzionas. GOAL: Generating 4D whole-body motion for hand-object grasping. In *Conference on Computer Vision and Pattern Recognition (CVPR)*, 2022. 2
- [43] Guy Tevet, Sigal Raab, Brian Gordon, Yonatan Shafir, Daniel Cohen-or, and Amit Haim Bermano. Human motion diffusion model. In *ICLR*, 2023. 2, 3, 4, 6, 7, 1
- [44] Sibotian, Minghui Zheng, and Xiao Liang. Transfusion: A practical and effective transformer-based diffusion model for 3d human motion prediction. *arXiv preprint arXiv:2307.16106*, 2023. 2
- [45] Ashish Vaswani, Noam Shazeer, Niki Parmar, Jakob Uszkoreit, Llion Jones, Aidan N Gomez, Łukasz Kaiser, and Illia Polosukhin. Attention is all you need. *Advances in neural information processing systems*, 30, 2017. 4, 1, 2
- [46] Jingbo Wang, Yu Rong, Jingyuan Liu, Sijie Yan, Dahua Lin, and Bo Dai. Towards diverse and natural scene-aware 3d human motion synthesis. In *CVPR*, 2022. 2
- [47] Zan Wang, Yixin Chen, Tengyu Liu, Yixin Zhu, Wei Liang, and Siyuan Huang. Humanise: Language-conditioned human motion generation in 3d scenes. *NeurIPS*, 2022. 2
- [48] Dong Wei, Xiaoning Sun, Huaijiang Sun, Bin Li, Shengxiang Hu, Weiqing Li, and Jianfeng Lu. Understanding text-driven motion synthesis with keyframe collaboration via diffusion models. *arXiv preprint arXiv:2305.13773*, 2023. 2
- [49] Yan Wu, Jiahao Wang, Yan Zhang, Siwei Zhang, Otmar Hilliges, Fisher Yu, and Siyu Tang. Saga: Stochastic whole-body grasping with contact. In *Proceedings of the European Conference on Computer Vision (ECCV)*, 2022. 2
- [50] Yiming Xie, Varun Jampani, Lei Zhong, Deqing Sun, and Huaizu Jiang. Omnicontrol: Control any joint at any time for human motion generation, 2023. 2, 5
- [51] Sirui Xu, Zhengyuan Li, Yu-Xiong Wang, and Liang-Yan Gui. Interdiff: Generating 3d human-object interactions with physics-informed diffusion. In *ICCV*, 2023. 2, 4
- [52] Jianrong Zhang, Yangsong Zhang, Xiaodong Cun, Shaoli Huang, Yong Zhang, Hongwei Zhao, Hongtao Lu, and Xi Shen. T2m-gpt: Generating human motion from textual descriptions with discrete representations. In *CVPR*, 2023. 2
- [53] Mingyuan Zhang, Zhongang Cai, Liang Pan, Fangzhou Hong, Xinying Guo, Lei Yang, and Ziwei Liu. Motiondiffuse: Text-driven human motion generation with diffusion model. *ArXiv*, 2022.
- [54] Mingyuan Zhang, Xinying Guo, Liang Pan, Zhongang Cai, Fangzhou Hong, Huirong Li, Lei Yang, and Ziwei Liu. Remodiffuse: Retrieval-augmented motion diffusion model. *arXiv preprint arXiv:2304.01116*, 2023. 2
- [55] Xiaohan Zhang, Bharat Lal Bhatnagar, Sebastian Starke, Vladimir Gufov, and Gerard Pons-Moll. Couch: Towards controllable human-chair interactions. In *ECCV*, 2022. 2
- [56] Zihan Zhang, Richard Liu, Kfir Aberman, and Rana Hanocka. Tedi: Temporally-entangled diffusion for long-term motion synthesis. *arXiv preprint arXiv:2307.15042*, 2023. 2
- [57] Kaifeng Zhao, Yan Zhang, Shaoqi Wang, Thabo Beeler, and Siyu Tang. Synthesizing diverse human motions in 3d indoor scenes. *ArXiv*, 2023. 2

HOI-Diff: Text-Driven Synthesis of 3D Human-Object Interactions using Diffusion Models

Supplementary Material

A. Additional Details of Methodology

In Sec. 3 of our main paper, we presented the foundational design of each key component in our HOI-Diff pipeline. Here, we delve into an elaborate explanation of model architecture, learning objectives and additional details associated with each crucial component.

HOI diffusion model (HOI-DM). The Communication Module (CM) in HOI-DM is based on cross attention mechanism. Formally,

$$\tilde{f}^h = \text{MLP}(\text{Attn}(f^h \mathbf{W}_Q, f^o \mathbf{W}_K, f^o \mathbf{W}_V)), \quad (8)$$

$$\tilde{f}^o = \text{MLP}(\text{Attn}(f^o \mathbf{W}_Q, f^h \mathbf{W}_K, f^h \mathbf{W}_V)), \quad (9)$$

where $\text{MLP}(\cdot)$ denotes fully-connected layers, $\text{Attn}(\cdot)$ is the attention block [45], and $\mathbf{W}_Q, \mathbf{W}_K, \mathbf{W}_V$ are learned projection matrices for query, key, and value, respectively.

The training objective of this full model is based on reconstruction loss

$$\mathcal{L}_{hoi} = \mathbb{E}_{t \sim [1, T]} \|M_\theta(x_t, t, c) - x_0\|_2^2, \quad (10)$$

where x_0 is the ground truth of the HOI sequence.

Affordance prediction diffusion model (APDM). The affordance prediction diffusion model comprises eight Transformer layers for the encoder with a PointNet++ [33] to encode the object’s point clouds. The training objective of this diffusion model is also based on reconstruction loss

$$\mathcal{L}_{aff} = \mathbb{E}_{t \sim [1, T]} \|A_\theta(y_t, t, p, d) - y_0\|_2^2, \quad (11)$$

where y_0 is the ground-truth affordance data. p and d denote object point cloud and text description (prompt), respectively. A_θ represents the affordance prediction diffusion model.

Affordance-guided interaction correction. During the inference stage, it’s found that the predicted object contact positions may occasionally be inaccurately positioned, residing either inside or outside the object. To rectify this, we implement post-processing steps that replace these predicted contact points, denoted as y_0^o , with their nearest neighbors from the object’s point clouds. This adjustment aims to enhance the accuracy of the updated contact points, aligning them more closely with their actual positions on the object’s surface. However, employing these updated contact points directly for contact constraints, particularly in the absence of detailed human shape information, introduces

a new challenge. It can potentially lead to penetration issues within the contact area while reconstructing the human mesh in the final stage. To mitigate contact penetration, we adopt a method that recalculates points at a specified distance outward, perpendicular to the normal, originating from the object’s contact points.

As for smoothness term, we formulate it as

$$G_{smo} = \sum_{l=1}^{L-1} \|x_0^o(l+1) - x_0^o(l)\|^2, \quad (12)$$

where $x_0^o(l)$ is the predicted 6DoF pose of the object in the l -th frame.

B. Additional Details of Baselines

- **MDM^{finetuned}.** We finetune MDM [43] on BEHAVE dataset without considering the object motion.
- **MDM*:** We extend the original feature dimensions of the input and output processing in MDM [43] from D^h to $D^h + D^o$, enabling support for HOIs sequences. The model is trained from scratch on BEHAVE dataset [3].
- **PriorMDM*:** The proposed approach for dual-person motion generation employs paired fixed MDMs [43] per individual to ensure uniformity within generated human motion distributions. This design leverages a singular ComMDM to coordinate between the two branches of fixed MDM instances, streamlining training and maintaining consistency across generated motions. Given that both branches are based on MDM that pretrained on human motion datasets, direct utilization of them for human-object interactions in our task is infeasible. We maintain one branch dedicated to humans, leveraging pretrained weights, while adapting the input and output processing of another branch specifically for generating object motion. Following this, we fine-tune the human MDM branch while initiating the learning of object motion from scratch within the object branch. Eventually, we integrate ComMDM to facilitate communication and coordination between these distinct branches handling human and object interactions.

To ensure fair comparisons, all the above baselines as well as our own models are all trained on BEHAVE for 20k steps.

C. Additional Details of Evaluation Metrics

For detailed information regarding metrics employed in human motion generation, including *FID*, *R-Precision*, and

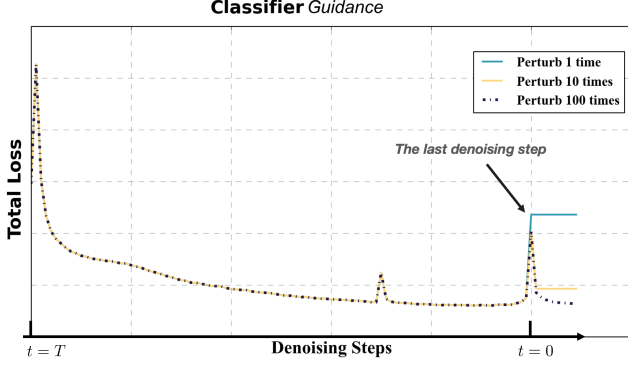


Figure 7. Effect of different number of perturbations in the final denoising step.

Diversity, we refer readers to [10, 43] for comprehensive understanding.

Expanding on the concept of *Contact Distance*, we utilize the *chamfer distance* metric to quantify the closeness between human body joints and the object surface. This computation leverages ground-truth affordance data that includes human contact labels and object contact points,

$$\text{ContactDistance} = \frac{1}{L} \sum_l^L CD(\hat{x}_l^h, \hat{p}_l), \quad (13)$$

where \hat{x}_l^h represents two human contact joints at the l -th frame, indexed according to ground-truth contact labels. Additionally, \hat{p}_l denotes two object contact points derived from the object motion x_l^o at frame l , also indexed based on ground-truth information. CD denotes the *chamfer distance*.

D. Implementation Details

Both our HOI-MDM and APDM are built on the Transformer [45] architecture. Similar to MDM [43], we employ the CLIP model to encode text prompts, adhering to a classifier-free generation process. Our models are trained using PyTorch [30] on 1 NVIDIA A5000 GPU. We set control strength of guidance as $\tau_1 = 1$, $\tau_2 = 100$, and $\Sigma_t = \min(\Sigma_t, 0.01)$.

Model architecture. Both the HOI-DM and APDM architectures of HOI-Diff are based on Transformers with 4 attention heads, a latent dimension of 512, a dropout of 0.1, a feed-forward size of 1024, and the GeLU activation [12]. The number of learned parameters for each model is stated in Tab. 3.

Training hyperparameters. Our training setting involves 20k iterations for the HOI-MDM and 10k iterations for the APDM model. These iterations utilize a batch size of 32

Table 3. The number of learned parameters of our two core architectures.

Model	HOI-DM	APDM
Parameters ($\cdot 10^6$)	8.82	38.92

and employ the AdamW optimizer [26] with a learning rate set at 10^{-4} . We use $T=1000$ and $N=500$ diffusion steps in HOI-DM and APDM, respectively.

E. Inference Time

In Tab. 4, we provide the inference times for both baselines and our full method, including its key components. All measurements were conducted using an NVIDIA A5000 GPU. Training an additional model for affordance information and using classifier guidance for interaction correction do contribute to increased inference costs. However, despite the longer inference time, our complete method notably enhances the accuracy of 3D HOIs generation.

Table 4. **Inference Time.** We report the inference time for baselines, our full method, and its key components.

Method	MDM*	PriorMDM*	Ours (Full)
Time (s)	32.3	38.6	118.0
Component	APDM	HOI-DM	Interaction Correction
Time (s)	24.2	46.4	47.4

F. Additional Ablation Studies

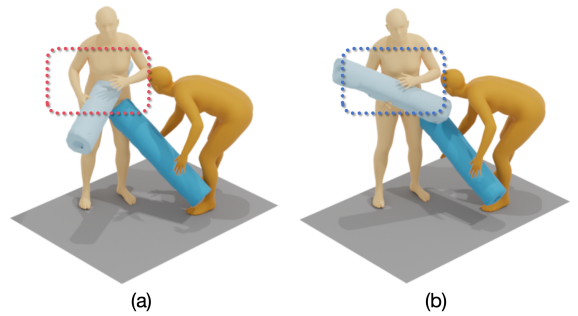


Figure 8. Effect of different control strengths for classifier guidance. (a) We use equal strengths of $\tau_1 = 1$, $\tau_2 = 1$ to perturb the predicted mean of human motion and object motion, respectively. (b) We use different strengths of $\tau_1 = 1$, $\tau_2 = 100$ for the perturbation. We can see that different strengths work better.

Different perturbing times in classifier guidance. As discussed in Sec. 3.4, in the later stage of classifier guid-

Table 5. Examples of our annotated textual descriptions for the BEHAVE dataset generated by GPT-3.5.

Object	Textual Descriptions
<i>backpack</i>	A person is carrying the backpack in front.
	The person is raising a backpack with his right hand.
	The person at the front presently has control over the backpack.
<i>chairwood</i> (<i>wooden chair</i>)	A person is using the chairwood for sitting.
	The person is propelling the chairwood on the ground.
	Someone is hoisting a chairwood by his left hand.
<i>tablesquare</i> (<i>square table</i>)	A person is lifting the tablesquare, utilizing his left hand.
	Someone is clutching onto a tablesquare from the front.
	An individual is moving the tablesquare back and forth.
<i>boxlong</i> (<i>long box</i>)	A person is gripping the boxlong from the front.
	A person is raising the boxlong using his left hand.
	Someone hoists the boxlong with his left hand.
<i>toolbox</i>	Someone is grasping the toolbox upfront.
	The person has a firm hold on the toolbox with his right hand.
	A person is gripping the toolbox with his left hand.
<i>yogaball</i>	A person is shifting a yogaball back and forth on the floor using his hands.
	The person is occupying a yogaball.
	A person is employing an yogaball to engage in an upper body game.

ance, diffusion models tend to strongly attenuate the introduced signals. Therefore, we iteratively perturb the predicted mean of motion for K times at the final denoising step. In Fig. 7, we present the ablation results, illustrating the impact of different numbers of perturbations. Notably, we observe that employing 100 perturbations leads to re-convergence and yields the desired results.

Different guidance strength. As detailed in Sec. 3.4, we employ distinct control strengths for classifier guidance, considering the varying feature densities in predicted human and object motion. Rather than employing equal control strengths, we opt to assign a higher control strength to object motion, allowing it to closely align with human contact joints, as illustrated in Fig. 8.

G. Annotation for BEHAVE Dataset

Textual Descriptions. In Tab. 5, we showcase a selection of our annotated textual descriptions for the BEHAVE dataset [3]. Initially, we manually annotate the interaction types and the specific human body parts involved, delineating actions like “lift” associated with the “left hand” or “hold” involving “two hands”. Subsequently, to generate complete sentences, we leverage the capabilities of GPT-3.5 to assist in formulating the entirety of the description.

Affordance Data. Our affordance data includes human contact labels, object contact points, and object state labels. We employ *chamfer distance* to measure the distance between all human body joints and object surface points. Following a predefined distance threshold $\gamma = 0.1$, we identify the two nearest contact points on the object surface corresponding to the 8 primary human body joints. In scenarios involving single-joint interactions (e.g., *lift a box using the left hand*), we index only one human contact joint and pair it with two object contact points sharing the same position. Subsequently, we derive the human contact labels by encoding the indexes of contact joints into an 8-dimensional vector represented by binary values. Finally, we manually assign binary labels to denote the object state.

H. Supplementary Video

Beyond the qualitative results presented in the main paper, our supplementary materials offer comprehensive demos that provide an in-depth visualization of our task, further showcasing the effectiveness of our approach.

In these demonstrations, we highlight the better performance of our method, HOI-Diff, in producing diverse and realistic 3D HOIs while maintaining adherence to physical validity. Notably, the visualizations show that HOI-Diff consistently generates smooth, vivid interactions, accurately capturing human-object contacts.

Additionally, we present the visual ablation results and emphasize the significance and effectiveness of our affordance-guided interaction correction, underscoring its substantial impact on improving the overall performance and quality of the generated 3D HOIs.